Essays in Biochemistry (2021) **65** 67–79
https://doi.org/10.1042/EBC20200015

PORTLAND PRESS

Review Article

Challenges of analysing stochastic gene expression in bacteria using single-cell time-lapse experiments

Georgeos Hardo and Somenath Bakshi

Department of Engineering, University of Cambridge, Cambridge, United Kingdom

Correspondence: Somenath Bakshi (sb2330@cam.ac.uk)

Stochastic gene expression causes phenotypic heterogeneity in a population of genetically identical bacterial cells. Such non-genetic heterogeneity can have important consequences for the population fitness, and therefore cells implement regulation strategies to either suppress or exploit such heterogeneity to adapt to their circumstances. By employing time-lapse microscopy of single cells, the fluctuation dynamics of gene expression may be analysed, and their regulatory mechanisms thus deciphered. However, a careful consideration of the experimental design and data-analysis is needed to produce useful data for deriving meaningful insights from them. In the present paper, the individual steps and challenges involved in a time-lapse experiment are discussed, and a rigorous framework for designing, performing, and extracting single-cell gene expression dynamics data from such experiments is outlined.

Stochastic gene expression and non-genetic heterogeneity in bacteria

Gene expression in cells is inherently noisy since it involves diffusion-limited collisions between low copy number molecular species. For instance, if a particular gene exists in a single copy and has its operator regulated by a transcription factor (TF) also existing in very low copy numbers ($\lesssim$10 [1,2]), then the probabilistic nature of the successful binding events will cause the gene to stochastically transition between 'on' and 'off' states (Figure 1A). Therefore the 'state' of the gene will be intrinsically noisy, even if the copy numbers of the gene and the TF are kept fixed (as the TF binds, unbinds, diffuses, searches, and rebinds). Even if the copy number of genes, RNA polymerases (RNAPs), and ribonucleases are kept fixed, transcript levels will fluctuate due to the random collisions between RNAP and the active gene's promoter, and between transcripts and the ribonucleases (Figure 1B). In a similar way, random birth and death events of proteins will lead to noisy protein abundances even if the abundances of mRNA, ribosomes, and proteases are kept fixed (Figure 1C). Therefore each step in the gene expression process is *intrinsically* noisy.

The connections between every step in gene expression cause the noise to be propagated from one system to another, thus introducing *extrinsic* noise in each step [3]. For example, random switching of a gene's active state leads to extrinsic noise in the mRNA abundance, and the noise in mRNA levels is propagated into the noise in the protein copy numbers (Figure 1D). This propagated noise is termed as the *extrinsic* component of the noise. Since every gene expression process in the cell shares the same pool of RNAP, ribosomes and degradation machinery (such as nucleases or proteases), there is a connectedness amongst all processes in the cell through which noise propagates. Moreover, the gene regulatory network connects specific genes together and provides additional specific modes of noise propagation. Together these cause the entire transcriptome and proteome to fluctuate across the population and over time.

There are additional contributors to the variability of gene expression in cells. The noisy nature of cell growth and the variability in the division times creates daughters of different sizes (Figure 1E).

Received: 15 October 2020
Revised: 02 March 2021
Accepted: 04 March 2021

Version of Record published:
16 April 2021

Essays in Biochemistry (2021) **65** 67–79
https://doi.org/10.1042/EBC20200015

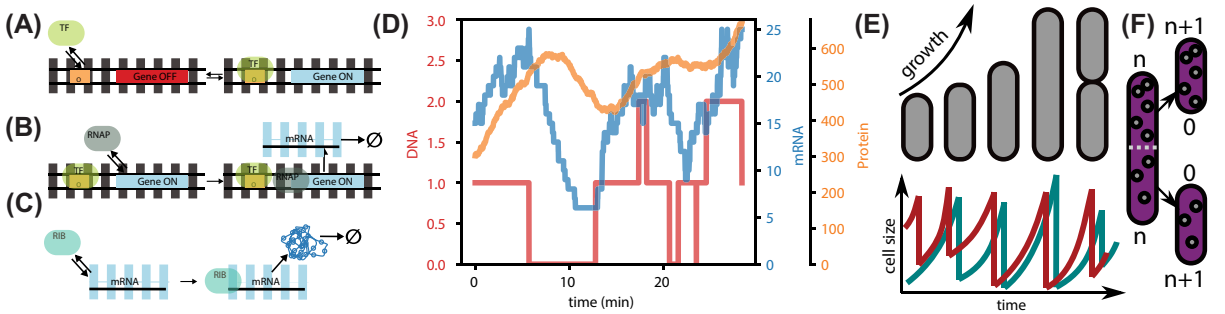

Figure 1. Sources of non-genetic heterogeneity in bacteria

(**A**) A TF binds to the operator site (O) and activates a gene with a certain probability. (**B**) For an active gene, RNAP can bind to the promoter, and the probability of activation is determined by the promoter strength [7]. Once this occurs, a transcript is produced and exists until it is degraded by ribonucleases. (**C**) Transcripts bind to ribosomes (RIB) and translation is initiated to form a protein, which itself degrades or is diluted. (**D**) An example time trace of the system was modelled by the Gillespie Algorithm [8]. The copy number of active genes fluctuates and the mRNA levels adjust to it depending on the relative timescales of changing gene activity and mRNA lifetime. Similarly, the protein levels adjust to the fluctuation in the mRNA, but with a certain amount of lag due to their slow degradation. (**E**) Division times are heterogeneous, leading to cell cycle desynchronisation within a colony. Moreover, this introduces heterogeneity into the sizes of newborns. (**F**) Molecules are partitioned into daughter cells based on a number of factors, such as their concentration, excluded cell volume etc. [9]. Moreover, successive divisions age the pole of the cell, causing it to accumulate damage (age shown above each pole). Poles accumulating age are the method by which we can describe the age of a single cell.

This leads to cell cycle heterogeneity and desynchronisation across the population. Moreover, random partitioning of intracellular resources during cell division leads to further post-divisional heterogeneity (Figure 1F) [4]. In bacterial cells, due to their small size and consequently having a lower copy number of individual mRNA or protein species, the noise from all of these sources is quite significant. This leads to non-genetic heterogeneity in a population of genetically identical cells, and can contribute significantly to the population's fitness [5]. Bacteria implement different regulatory strategies, both to suppress noise when a reliable response is required [6], and to exploit it when variability can improve the fitness of the population overall [5]. In order to understand these regulatory mechanisms, the noise in gene expression needs to be rigorously characterised and analysed.

Time-lapse experiments for studying stochastic gene expression

Even though snapshot studies can encapsulate the full distribution of a population's heterogeneity, they are not suitable for analysing the sources of noise, since it is difficult to isolate and eliminate other confounding factors such as cell-cycle heterogeneity, or the age distribution of cells [10]. Additionally, the snapshot measurements contain no information about fluctuation dynamics. As shown in Figure 2A, two species with an almost identical distribution of copy numbers can have very different fluctuation dynamics. This can be distinguished from time-lapse imaging and comparing the decay time of the corresponding autocorrelation functions (Figure 2B,C). These dynamics play an important role in population heterogeneity because while fast fluctuations can be easily time averaged, the slow fluctuations can persist for long enough to establish developmental states. Analysing fluctuation dynamics can also enable us to identify contributions and connections between sources of noise through analysis of their correlation [11]. For example, even though one can use two copies of the same promoter to control the expression of two different fluorescent proteins (FPs; also known as the dual reporter system) to help identify the intrinsic and extrinsic contributions to noise [12], one needs time-lapse studies of dual-reporter systems to accurately quantify the individual noise contributions to the total [11]. In this review, attention is focussed to fluorescence time-lapse microscopy for analysing noise dynamics. These experiments involve the design and construction of fluorescent reporters, placing cells containing these reporters into suitable imaging platforms, monitoring the expression dynamics using time-lapse microscopy, and computationally analysing the micrographs to quantify the single-cell fluctuation dynamics. Each of these steps and the challenges in using them are described, while guidelines for a rigorous framework for designing such experiments is also provided.

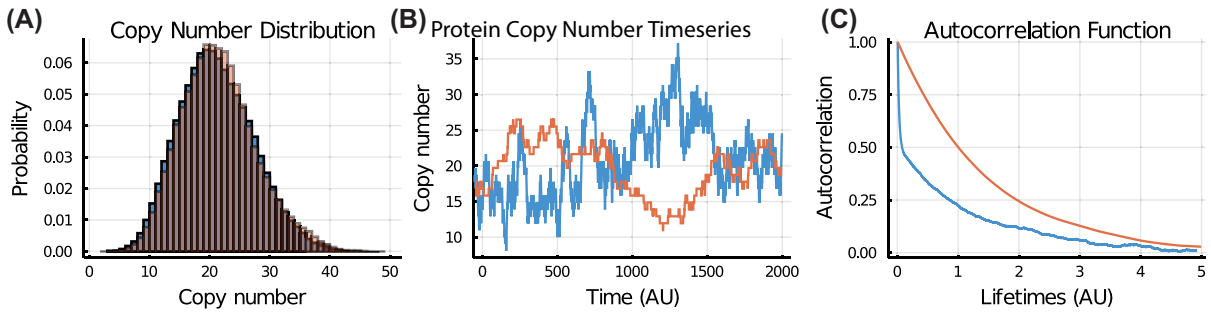

Figure 2. Analysis of stochastic gene-expression using snapshot and timelapse measurements

This figure shows distributions, dynamics, and autocorrelations of a fluctuating molecular species (e.g., mRNA or protein), but with rate constants which differ by an order of magnitude (simulated using the Gillespie algorithm). (**A**) Shows how even with different rate constants, the copy number of these species are almost identically distributed, making them impossible to tell apart by this measurement alone. Moreover, as is shown in (**B**), their fluctuations appear to look similar. This means that snapshot measurements would not tell them apart. (**C**) Shows that only by comparing each trace's autocorrelation function can one determine the true difference in the timescales of each species' dynamics. Thus the autocorrelation function can be said to capture the structure of the noise [13] and the timescale of the system's memory.

Reporters for time-lapse studies of gene expression

In order to quantify noise in the steps of gene expression, the absolute abundances of mRNA and protein need to be measured. Currently, the only reliable measurements for directly quantifying abundances of mRNA is single-molecule Fluorescence *In Situ* Hybridisation (FISH), where one uses fluorescently labelled nucleic acid probes to image spots for each mRNA and count them [14]. However, this method only works for fixed cells, and therefore is not applicable for time-lapse studies. Fluorogenic RNA aptamers, like Spinach, which bind to the mRNA of choice [15] are possible live-cell alternatives. However the most popular approach for quantifying transcriptional dynamics is to use FP-based *transcription reporters*, which are constructed by inserting an FP cassette under the control of the gene of interest's cognate promoter, often placed on a plasmid [16]. Since plasmid copy number itself may fluctuate [4,9,17], and the additional sites on the plasmids may titrate away low-copy TFs, placing the *promoter–fp* fusions on a single copy vector [18,19] is recommended, and directly integrating into the chromosome (preferably near the gene of interest's locus) is even more preferable to avoid mismatches in copy number [20]. For measuring translational dynamics, FP reporters are fused to the protein of interest to make translational reporters and the abundances can be quantified via imaging. A comprehensive discussion of the relevant design strategies are discussed by Snapp and Chen et al. [21,22].

In order to reliably track the dynamics of transcription and translation, the FP reporters need to rapidly adjust to transcript and protein levels. The slow maturation time of most FPs (∼1 h) [23] renders them unsuitable for tracking fluctuations dynamics, since maturation delay lags and time-averages the noise. In tracking the fluctuation dynamics and quantifying the expression noise of a protein, the slow dynamics of its reporter will not be able to reliably track the dynamics of fluctuations in mRNA level, since it lags and time-averages the noise. This will lead to underestimation of the noise and alteration of the dynamics. Maturation therefore acts as a low-pass filter over the fluctuation dynamics. Additionally, the slow maturation of the reporters makes only a fraction of the reporters appear bright and detectable, since they appear slowly with a distributed delay while being diluted by growth. Therefore, such reporters can under-report the abundances. To minimise these issues fast-maturing FPs are being engineered such as mVenus, with a maturation time of ∼2 min [24]. To correlate expression dynamics from more than one gene, one needs to make sure that the spectral overlap between the reporters is low. Other fast-maturing proteins (mCerulean: 6.6 min, SCFP3A: 6.4 min, mGFPmut2: 5.6 min, mGFPmut3^{d}: 4.1 min) have also been characterised to address this problem, and a full list is available in [25], however no suitably fast-maturing variant of RFP is yet available. Alternatively, one can use self-labelling proteins such as Halo or SNAP-tag that do not suffer from similar maturation delay [26]. However, such tags are yet to be used for time-lapse imaging.

Platforms for time-lapse studies of gene expression

For measuring gene expression dynamics, cells containing transcription or translation reporters are placed in platforms and imaged over time. The imaging platforms need to have spatiotemporally uniform growth conditions, so that heterogeneities across the population and over time can be reliably quantified. Surprisingly, most of the imaging

Essays in Biochemistry (2021) **65** 67–79
https://doi.org/10.1042/EBC20200015

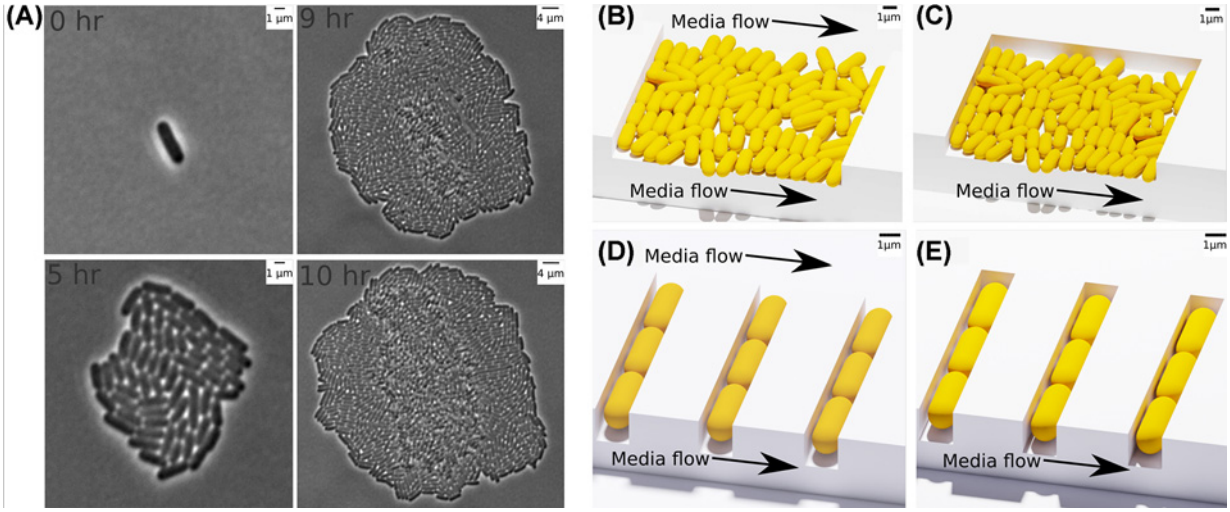

Figure 3. Different platforms for timelapse imaging of single cells

(**A**) An agarose-pad does not allow for long-term imaging, since the rod-like cells within the microcolony are confined to two dimensions until the colony transitions into 3D growth (as seen from the dark cells in the centre of this microcolony from t = 9 onwards). (**B**–**E**) Illustrative 3D models of imaging platforms for time-lapse single-cell imaging, drawn and rendered using Blender [29]. Top row: imaging platforms for two-dimensional growth. Bottom row: platforms for one-dimensional growth. (B) The two-dimensional microfluidic turbidostat with two sides open lets cells wash away to maintain a fixed population size. (C) This version lets cells wash away from one side only. Both of the devices in (B) and (C) keeps cells well-fed and confined to a monolayer throughout the experiment, but suffer from PSF artefacts in imaging due the tight packing of cells, and can have non-homogeneous nutrient availability across the device. (D) The one-dimensional single-celled chemostat enables tracking a single lineage without PSF artefacts, but suffers from limited residence time of individual cells in the trenches. (E) The one-dimensional analogue of the device above, also known as the mother machine, provides the longest measurements of individual cells. Note that the use of one-dimensional devices is limited to rod-like bacteria so that the cell growth occurs along the major axis of the device

platforms used in such experiments do not qualify for this. Traditionally, these measurements are done by seeding cells on to an agarose-pad, and imaging them as they grow into a microcolony (Figure 3A). Single cells are computationally tracked within the growing microcolony, and the reporter signal within each cell is quantified to analyse the fluctuation dynamics [27]. However, nutrient availability within the agarose-pad is not uniform, and so cells in different positions in the microcolony experience different environmental conditions [28]. The measurement of fluctuation-dynamics is also unreliable, since the nutrient profile also changes over time. Moreover, in-plane growth of cells in the monolayer colony eventually starts to transition into vertical growth (Figure 3A) [28]. Additionally, the dense-packing of cells results in 'bleed-through' of light from one cell to the other due to the finite size of the point-spread function (PSF; detailed discussion in the section entitled *Analysis of time-lapse data of stochastic gene expression*, below) and introduces imaging artefacts.

Microfluidic devices have been developed that mitigate some or most of these problems. Most of the devices used for time-resolved imaging of single cells maintain a monolayer of cells, and thus allow for the growth of cells in either one or two dimensions. In order to solve the issue of finite experiment time which arises from agarose pads, devices which allow newborn cells to be washed away over time have been developed. Mather et al. [30] developed two-dimensional microfluidic turbidostats which allow for monolayers of cells to grow and get washed from either two sides (Figure 3B) or from one side (Figure 3C). These types of devices have been employed for high-throughput gene expression studies [31]. However, fluorescent measurement in such devices will still suffer from significant PSF bleed-through artefacts, which is later described being the effect of the diffraction caused by the microscope's optics, resulting in artificial spill-out of intensity to neighbouring cells.

The two aforementioned devices have one-dimensional analogues. The one-dimensional chemostat contains single-file cells in narrow trenches and has both ends open [32]. This device enables monitoring single cells without altering their age distribution and without experiencing significant confounding effects of PSF bleed-through (Figure 3D). However, this device – by virtue of preserving age distribution – cannot trap single cells for long-term study. To probe the dynamics of a particular cell over many generations, one needs to use the mother machine [33]

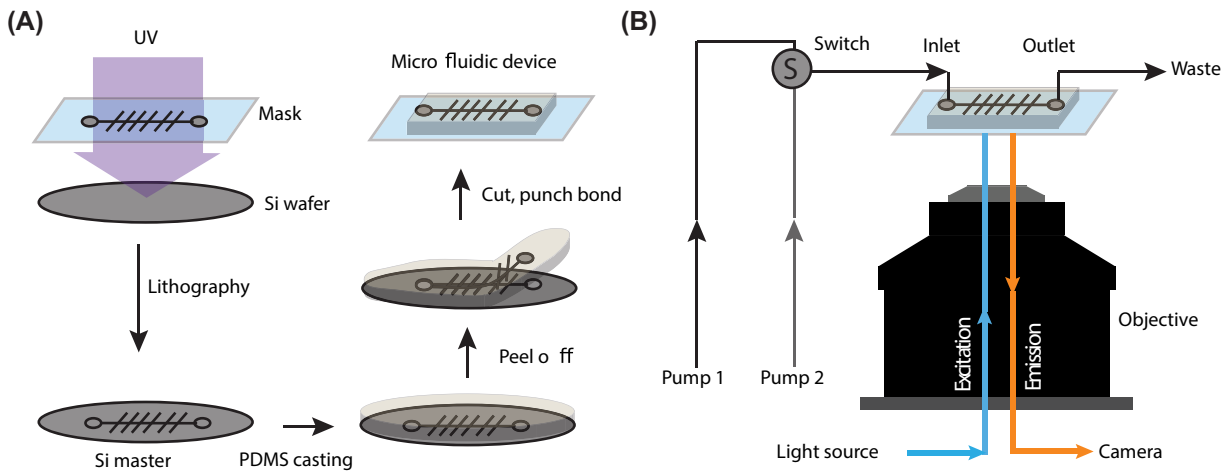

Figure 4. An overview of the process of creating microfluidic devices for single-cell analysis, and using them in an imaging setup

(**A**) The general workflow for producing a microfluidic device – patterning a photoresistant-coated Si wafer using photo-lithography, using the patterned Si master for casting polydimethylsiloxane (PDMS) moulds, cutting chips out of this PDMS mould and bonding it to coverslips to fabricate the device. (**B**) The microfluidic device preloaded with cells is connected the media flow and placed on an inverted microscope. Cells in this device are imaged through a high-resolution objective, and media flow is controlled using pumps and flow-switches.

(Figure 3E) where the 'mother' cells stay at the closed end of the trench for many generations while its progeny are washed away. Norman et al. were able to track *Bacillus subtilis* for 700 generations in the mother machine [34]. Versions of this device that enable the tracking 130 000 cells in parallel for hundreds of generations have recently been produced [35]. The trenches of the mother machine must have proper dimensions to allow for nutrient diffusion to the mother cell, and various trench geometries need to be sampled to determine optimal sizes for varying conditions [35].

While this device does not maintain the consistent age 103 distribution of the population, it enables one to study impacts of ageing on cellular fitness [36,37], which can introduce non-genetic heterogeneity into populations of cells.

It should be noted that the aforementioned microfluidic devices are only suitable for studying rod-like bacteria over multiple generations, because these strains grow in plane, and their growth can also be confined to one dimension. However, adapted versions of these devices have been used to study growth and susceptibility of both cocci and rod-like bacteria towards antimicrobials [38]. Since the rod-like shape (spherocylinder) is the default shape of bacteria, and is the shape of the canonical Gram-negative and Gram-positive bacteria, *Escherichia coli* and *B. subtilis*, where most gene expression studies are conducted, we keep the discussions of experimental design and analysis pipelines in the next sections limited to this shape. The general approach and framework should still be valid for cells of different shapes as long as corresponding devices enable single-cell studies satisfying the criteria discussed in this section.

Experimental setup for time-lapse imaging of single bacterial cells

As discussed above, microfluidic devices are the most suitable platform for time-lapse imaging of single bacterial cells, and therefore the following sections' discussions are limited to experimental setups and analysis pipelines for imaging cells in microfluidic devices. The manufacturing process of microfluidic devices is relatively simple and enables the fabrication of devices with any intended layout. When designing a layout, one should consider nutrient homogeneity, imaging artefacts, and required throughput of the experiment. The layout of the chip is designed in a computer-aided design (CAD) software package and printed on to a mask (either plastic or chrome, depending on the desired feature size). Figure 4A shows the general steps involved in the production process of a microfluidic device from this mask. A comprehensive account of the relevant technical details is provided in these review articles [39,40]. Prior to the experiment, cells are loaded in the microfluidic device which is placed over the microscope objective for imaging. Needles are inserted into the inlet and outlet of the device, which are connected to a flow control system which modulates the media flow through the device, and the addition of any desired liquid [41]. Inverted

Essays in Biochemistry (2021) **65** 67–79
https://doi.org/10.1042/EBC20200015

microscopes with high-resolution objectives are used for imaging bacteria trapped in these devices. This enables simultaneous bright-field imaging through Kohler illumination, and fluorescence imaging using epi-illumination. Oil-based objectives offer higher resolution and sensitivity due to their higher numerical aperture, while air objectives provide flexibility and fast scanning speeds and can enable longer duration experiments since they do not suffer from the problem of oil drying over time. A schematic of the imaging and flow control setup is shown in Figure 4B.

For time-lapse single-cell experiments, along with the fluorescent image of the reporter, one can also collect an additional bright-field image of the cell itself. For bacteria, phase-contrast imaging produces better contrast than differential interference contrast (DIC) or conventional bright-field imaging. The phase-contrast image can be used to identify the boundaries of single cells in every image, so that the intensity and spacial properties of the fluorescent signal within can be quantified. Alternatively, one can use a strong fluorescent signal from constitutively expressed FPs to produce a bright fluorescent image of a cell which can also be used for segmentation. Phase-constrast may be preferable for this task, since expression of the fluorescent segmentation marker can introduce a growth burden on the cell [42]. Additionally, for high time resolution imaging, constant exposure with the excitation light, and subsequent photo-bleaching will result in the production of reactive oxygen species (ROS) causing photo-toxic damage to the cell [43]. Phase-contrast microscopy does not require modifying the cell to introduce a marker and thus reduces any photo-toxic effects and expression burden. However, the scanning time of the device also limits the time resolution, and therefore one must strike the right balance between the required throughput, time resolution, while minimising phototoxicity. The high-throughput nature of time-lapse experiments in microfluidic devices [33,35,31] coupled with the long-term imaging at high time resolutions generates a vast amount of data. Analysing these data by hand is an impossible task, and accurate automated analysis pipelines are the only option. We discuss the automated approaches towards this in the following section.

Analysis of time-lapse data of stochastic gene expression

Image formation

Before discussing image analysis, a brief overview of image formation is helpful, since image analysis is simply the reverse of image formation; going from the image back to the object's properties. For fluorescence microscopy, one uses a light-source (LEDs or LASERs) to excite fluorescent emitters (reporter probes) in the cell placed in the imaging platform. Upon excitation, they emit red-shifted light, part of which is collected through the objective lens and focused on the camera to form an image. The light microscope is, however, a diffraction limited device, and so the image collection process generates artefacts [44]. Fluorescent or transmitted light from the object plane passes through the microscope's optics to reach the image plane in the camera, but gets diffracted in the process. This causes the light to gets distributed beyond its point of origin, causing a point to appear as a blurry spot, called the PSF. The PSF causes light from any object to spread beyond its boundary, and thus blurs the image.

The phase-contrast point spread function has alternating phases 5, causing it to have alternating bright and dark concentric rings. This limits our abilities to segment cells from an image, especially when they are trapped in microfluidic devices. However, apodised phase-contrast objectives have mitigated this issue significantly [45,46]. Apodised objectives have been used to image the growth and division of bacterial cells with 1 min resolution, giving >20 data-points per cell-cycle of fast-growing bacteria, enabling detailed analysis of size-regulation principles [35]. The size of the fluorescent PSF (theoretically described by the Airy formula, which depends on the wavelength of emitted light) determines the extent to which light spreads from a cell full of fluorescent emitters, and can introduce artefacts in quantifying intensity distribution. As mentioned above, one can also use fluorescent images for segmenting cells. When using fluorescent imaging, due to the photo-toxic effects, one must reduce the imaging frequency in order to minimise the incident radiation on the cells. This allows cells to dilute any photo-toxic products generated from imaging before it starts to overly damage their health.

Image segmentation: identifying individual cells in a frame

Analysis of time-lapse data begins with cell segmentation. This is the process of drawing pixel masks over cells so that they are separated from the background. The input data are an image of the cells and the output of this process is a binary mask, where cells have a pixel value of 1, and the background has a value of 0. If cells are growing within close proximity of one another, such as on agarose-pads (Figure 5A) or in a device such as a microfluidic turbidostat [31,47] (Figure 5B,C), then the challenge is to resolve cells from each other. Oufti (which recently superseded MicrobeTracker) [48–50], is an extensive suite that can generate accurate masks for cells from a tightly packed cluster. Segmentation of single cells from images of mother machine experiments should be straightforward, since cells are organised in nicely packed linear colonies. However, the phase-contrast images of cells in such devices have lower

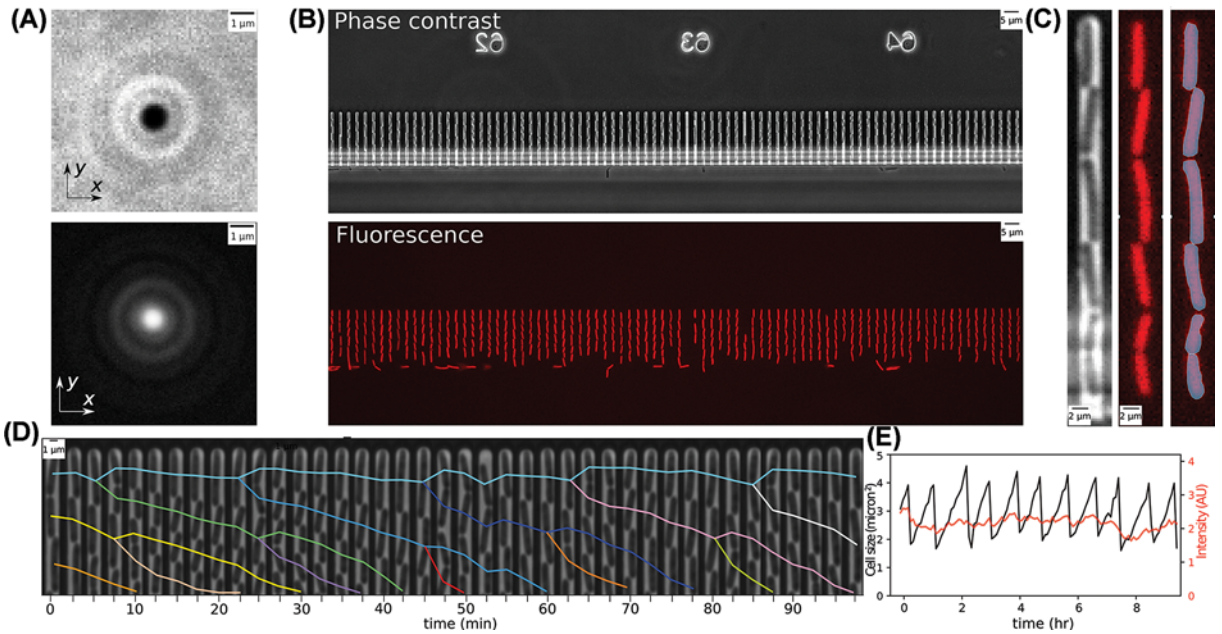

Figure 5. Imaging modalities and image analysis of mother-machine experiments

(**A**) Shows a real phase-contrast PSF and a real fluorescence PSF (enhanced contrast for visualisation). These were captured by imaging 100-nm fluorescent beads on a Nikon Ti-2 using a 60× phase-contrast air objective with NA = 0:95 (and at $\lambda = 610$ nm for the fluorescence PSF) at optimal focus. (**B**) Besides each PSF is an image of a field of view of cells in a mother machine, captured in phase-contrast (top) and mCherry fluorescence (bottom). Each image inherits its features as a result of the point spread function of the imaging modality. The phase contrast image's unchanging features such as the trenches and labels make it good for drift correction, while the fluorescence image allows one to very easily isolate cells. (**C**) An example of a single trench from the phase-contrast image, the corresponding fluorescence image, and the fluorescence image with the pixel mask overlaid on top. (**D**) Kymograph of cells in a single trench in mother machine with lineage tracks showing division events and cell positions. (**E**) Cell size and average fluorescence intensity of a single cell in mother machine over time.

contrast than usual, due to close proximity of the trench wall (Figure 5B). While fluorescence images may sometimes capture the structure of the imaging platform from out of focus light, background noise etc., this is usually dim in comparison with the signal from the cells. Phase-contrast imaging makes the platform an actual feature of the image (as can be seen in Figure 5B). Additionally the artefacts caused by the phase-contrast PSF (Figure 5A) cause these nearby cells or platform boundaries to interfere with the image of cells of interest, reducing their contrast significantly (especially at lower magnifications).

There are algorithms that provide reliable segmentation with traditional tools. Table 1 contains a list of currently available tools used for segmentation of mother machine images. Of note are deep learning-based tools. These promise to alleviate problems with low segmentation accuracy, especially for low-quality datasets. By training a model specific to the data, or specific to datasets which are similar, the model can: be robust to changes in contrast, be specific to cell shape, recognise regions where cells touch each other, and recognise the walls of the mother machine. This should enable higher segmentation accuracy. The majority of published deep learning-based frameworks are based around the U-net architecture [51]. This convolutional neural network (CNN) architecture is easily trained with relatively small amounts of data, can be quite robust to transformations in image shape, orientation, intensity etc. [52]. Since the performance depends on the quality and quantity of training data, these programs often have low transferability, can contain bias and artefacts from the training data, and require human curated data for training (which is time-consuming).

Cell tracking: identifying individual cells across frames

Once cells are identified, they need to be connected across frames. This produces a time-series of cellular properties (size, width, fluorescence intensity). Cell tracking is the process of keeping track of the same cell between time-frames. Lineage tracking refers to identifying the ancestral tree of cell lineages across the experiment. Figure

Essays in Biochemistry (2021) **65** 67–79
https://doi.org/10.1042/EBC20200015

Table 1 Table showing a list of currently used tools for segmenting and tracking cells of micrographs of microfluidic images

Tool	Usecase	Notes	Reference
BACMMAN	Segmentation + tracking	Contains several tracking algorithms	[54]
DeLTA	Segmentation + tracking	Separate networks for segmentation and tracking	[55]
DistNet	Segmentation + tracking	Single network for joint tracking and segmentation	[56]
MM3	Segmentation + tracking	Separate networks for segmentation and tracking	[57]
MMHelper	Segmentation + tracking	Multiple hypothesis tracking	[58]
MoMA	Segmentation + tracking	Bayesian approach to tracking	[59]
Oufti and Microbe Tracker	Segmentation + tracking	Also suitable for agarose-pad and 2D microfluidic devices	[50,31]
Parametric max-flow	Segmentation + tracking	Joint tracking + segmentation	[60]
pyStackReg	Image registration	Python implementation of StackReg/TurboReg	[61]
registrationEstimator	Image registration	A MATLAB tool	[62]
StackReg/TurboReg	Image registration	Used through ImageJ	[63]

Tools for image registration are also included.

5D gives a hand-drawn example of this. Most cell-tracking or lineage tracking approaches rely on connecting cells between frames according to spatial 183 proximity and the history of their size and shape. Therefore, it is important that the relative position of cells within the image changes only due to growth, not due to image drift. If there is significant drift between frames, 'drift correction' can eliminate it. For phase-contrast images of microfluidic platforms, static features, such as the structure of the PDMS devices can be used as reference markers for drift correction using image registration/template matching algorithms. Table 1 contains some image-registration tools which are commonly used to drift-correct time-series micrographs. We note here that, in a device such as the mother machine, where cells can only grow in one direction, drift correction is not a significant problem if one is unconcerned with lineage tracking. In this case mother cells can be easily extracted by passing their x and y coordinates through a clustering algorithm such as DBSCAN [53]. This clusters sets of xy coordinates into distinct groups, each representing a single mother cell. DBSCAN has been used in the past due to its ability to handle variable numbers of clusters, stage drift, and noise [35].

In general, tracking algorithms rely on the similarities and proximities of cell masks between frames in order to connect them as two images of the same cell in adjacent time-points. Often this is accomplished by a nearest neighbour search and maximising the overlap between masks in adjacent frames. We provide a summary of many of the tools which enable tracking in Table 1. DistNet's tracking errors are the lowest of any package discussed here, but MM3 and DeLTA also provide very good tracking above and beyond classical methods due to their trainable U-net architectures. It is important to note that all of these machine learning-based approaches require curated data in order to be trained. The generation of these data is time-consuming and must be done every time an experimental parameter is changed (such as the microscope, cell type, microfluidic device geometry etc.).

Quantifying intensities of fluorescent reporters within cells

Once the cells are segmented and tracked, the total fluorescence within their boundary can be quantified by summing up the intensities from the pixels within each mask in each frame. However, care must be taken to avoid issues with image shifts in different colours from lateral chromatic aberration in the optics. To minimise this effect, one can image multi-coloured fluorescent beads in the segmentation channel (phase-contrast) and the fluorescence channel (Figure 5) to accurately quantify the registry error between these each channel, and use image transformations to shift the pixel mask accordingly [64].

Once registry errors are minimised, one can quantify intensities withing cell masks. It is important to consider artefacts of diffraction for proper interpretation of the results. When using a fluorescence microscope, the PSF is convolved with the light coming from the sample to produce the image captured by the detector. In the simplest sense, the PSF 'blurs' the image, and is most commonly referred to when talking about the microscope's 'diffraction limit'. While the diffraction limit does not pose challenges for resolving single cells, the PSF does create a problem with quantifying single-cell intensities that occurs beyond the scale of the diffraction limit, due to PSF 'bleed-through'. Bleed-through corresponds to light which leaves the cell's true boundaries and 'leaks' into its surroundings. This

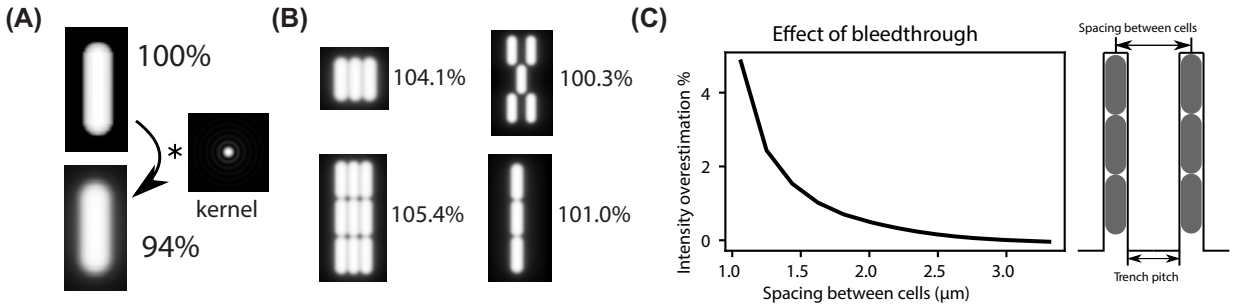

Figure 6. The effects of PSF bleedthrough on intensity measurements

(**A**) Cells were modelled as 3D spherocylinders and Monte Carlo sampling was used to place fluorescent emitters within their convex hull. The convolution of this synthetic cell with an ideal PSF demonstrates the intensity loss beyond the convex hull of the 2D projection of the cell in the image plane. (**B**) Cells were then placed in various positions to demonstrate the effects of bleed-through from neighbouring cells in various orientations. The percentage beside each image is the intensity of the central cell relative to its convolved solo intensity (relative to 94%). (**C**) These cells were then positioned within the geometry which one would expect of a mother machine (vertical lines of cells), and adjusted the pitch of these lines. The overestimation of the mother cell's intensity in a central trench based on trench pitch was then quantified. Emphasis should be placed on the fact that all these simulations involve image convolution with an idealised PSF modelled as an Airy disk with NA = 0:95, $\lambda = 610$ nm, n=1. Modelling this same experiment with defocussed PSFs produces significantly worse results, approaching 2–3× increases in intensity over-estimations, however because researchers are using different objectives, different depths of field etc. This model is the ideal case to show the theoretical best case scenario.

has two effects: a cell's brightness leaks into its immediate surroundings making its measured brightness within its pixel-mask lower than the true brightness. More importantly, it causes light to be 212 artificially assigned to other cells where it does not belong, and changes the distribution of intensities in the population.

In order to illustrate this effect simple numerical simulations were performed (Figure 6). Images of rod-shaped bacteria as spherocylindrical volumes containing uniformly distributed fluorescent (mCherry) emitters were simulated. The images of these cells were constructed through convolution with a typical PSF (modelled as an Airy disk [65]) of a fluorescence microscope with a 60× objective. The simulations show that when cells are in a densely packed colony, like in an agarose-pad or microfluidic devices such as those found in references [31,50], a significant amount (>5%) of light can come from the neighbours. These simulations were used to identify the contributions from each neighbour cell, which enables one to quantitatively estimate the expected bleed-through in each geometry. For devices like the mother machine, the 'mother-cell' (cell at the top of the trench that is tracked over time) primarily gets bleed-through from the cell below it (<1%). The mother machine device is flexible towards spacing trenches apart, and it has been possible to space the trenches far enough apart to eliminate the bleed-through from cells in nearby trenches [35].

The simulations also demonstrate that the bleed-though decreases rapidly as trenches are moved apart (Figure 6) and is negligible when cells are 3.5 micron apart, which is the lowest theoretical 'bleed-through limit' for this set parameters for reliably quantifying intensity from each cell. It is important to note here that these simulations are all performed with a PSF that is perfectly in focus, and since real cells have finite thickness, the broader out of focus PSF can actually lead to much more (2–3×) bleed-through compared with the theoretical estimations. One can get an intuition for the potential error by modelling the out of focus and asymmetrical PSFs for such simulations [65,66]. Using actual experiments, it has been found that a mother machine with 4 μm trench pitch leads to each cell receiving ∼2.5% of its total intensity from cells in adjacent trenches, which reduces down to ∼0.5% when they are 5 μm apart [35]. Therefore one must balance trade-offs (throughput vs bleed-through and linage size vs nutrient availability) by choosing appropriate dimensions.

Conclusions and future directions

In the present paper the steps which lead from the basics of a biological process of interest through to the measurements that enable its investigation have been laid out. A careful consideration of the underlying process dynamics and each of the steps involved in generating and analysing time-lapse data will guide both better experimental design, and data analysis pipeline design. It will also help to understand their limits. For example, an intuition for the

Essays in Biochemistry (2021) **65** 67–79
https://doi.org/10.1042/EBC20200015

abundances and fluctuation timescales can help the user in choosing FPs and designing reliable reporters and the type of measurements required. It is important to note here that monitoring fluctuation dynamics of reporters to infer the dynamics of the underlying process is still an indirect method and ideally one should quantify the absolute abundances of mRNAs and proteins in each cell. For quantifying fluctuation in mRNA levels, live cell measurements of mRNA copy number are needed [67], but with extensive orthogonal controls to make sure they are reliable. Quantifying proteins can be directly done using translational fusions, provided the reporter protein is fast-maturing, follows similar dilution timescales and does not interfere with the protein of interest's function. In order to analyse the dynamics of the reporter, it needs to be placed it in a platform that ensures a homogeneous environment and minimises PSF bleed-through. Molecular abundances can be quantified from fluorescence intensities using binomial segregation statistics at cell division [68]. Mother machine-like devices are particularly suitable for this, since one can observe many rounds of cell division under constant growth conditions. However, for molecules with low copy numbers ($\lesssim$10), when the fluorescence intensity becomes comparable or lower than the cellular autofluorescence, one has to rely on single-molecule counting. Currently, this the mother machine is not used for single-molecule counting, but we hope technical developments in this area will allow single molecule time-lapse measurements in mother machine-like devices. This will enable the combination of data on protein abundance fluctuations with data on copy number changes in the corresponding mRNA or TF. This would provide gold-standard data for analysing stochastic gene expression.

Summary

- Gene expression is noisy and is a major source of non-genetic heterogeneity.
- Time-lapse measurements are needed to characterise and analyse individual noise contributions in gene expression.
- Carefully designed reporters to study gene expression noise at the single-cell level are needed.
- The use of specific microfluidic devices for maintaining spatiotemporally invariant environment for imaging these reporters is suggested.
- Detailed consideration of the data-acquisition systems will help the user to design better data-analysis pipelines.
- The point spread function of a microscope can create severe artefacts in one's interpretation of the data, and should be considered in proper detail.

Competing Interests

The authors declare that there are no competing interests associated with the manuscript.

Funding

This research in the S.B.'s laboratory on studying stochastic processes in bacteria was supported by the Wellcome Trust Award [grant number RG89305]; a University Startup Award for Lectureship in Synthetic Biology [grant number NKXY ISSF3/46]; and the Ph.D. Studentship from BBSRC [grant number NMZR/077 (to Georgeos Harda)].

Open Access

Open access for this article was enabled by the participation of University of Cambridge in an all-inclusive *Read & Publish* pilot with Portland Press and the Biochemical Society under a transformative agreement with JISC.

Author Contribution

S.B. and G.H., both contributed equally to writing the review paper, creating the figures, and performing necessary simulations.

Acknowledgements

We thank Professor Johan Paulsson of Harvard University for the use of microscopy data collected in his lab by S.B. while there. We thank William Earley of Cambridge University for detailed feedback on the final manuscript. All figures included in the present paper are original and contain no third party material.

Abbreviations

CAD, computer aided design; FP, fluorescent protein; PDMS, polydimethylsiloxane; PSF, point-spread function; RNAP, RNA polymerase; TF, transcription factor.

References

1 Uphoff, S., Lord, N.D., Okumus, B., Potvin-Trottier, L., Sherratt, D.J. and Paulsson, J. (2016) Stochastic activation of a DNA damage response causes cell-to-cell mutation rate variation. *Science* **351**, 1094–1097, https://doi.org/10.1126/science.aac9786
2 Okumus, B., Landgraf, D., Lai, G.C., Bakhsi, S., Arias-Castro, J.C., Yildiz, S. et al. (2016) Mechanical slowing-down of cytoplasmic diffusion allows in vivo counting of proteins in individual cells. *Nat. Commun.* **7**, 1–11, https://doi.org/10.1038/ncomms11641
3 Paulsson, J. (2005) Models of stochastic gene expression. *Phys. Life Rev.* **2**, 157–175, https://doi.org/10.1016/j.plrev.2005.03.003
4 Huh, D. and Paulsson, J. (2011) Random partitioning of molecules at cell division. *Proc. Natl. Acad. Sci. U.S.A.* **108**, 15004–15009, https://doi.org/10.1073/pnas.1013171108
5 Rochman, N., Si, F. and Sun, S.X. (2016) To grow is not enough: Impact of noise on cell environmental response and fitness. *Integr. Biol.* **8**, 1030–1039, 1603.01579., https://doi.org/10.1039/C6IB00119J
6 Dublanche, Y., Michalodimitrakis, K., Kümmerer, N., Foglierini, M. and Serrano, L. (2006) Noise in transcription negative feedback loops: Simulation and experimental analysis. *Mol. Syst. Biol.* **2**, 41, https://doi.org/10.1038/msb4100081
7 Meng, C.A., Fazal, F.M. and Block, S.M. (2017) Real-time observation of polymerase-promoter contact remodeling during transcription initiation. *Nat. Commun.* **8**, 1–9, https://doi.org/10.1038/s41467-017-01041-1
8 Gillespie, D.T. (1977) Exact stochastic simulation of coupled chemical reactions. *J. Phys. Chem.* **81**, 2340–2361, https://doi.org/10.1021/j100540a008
9 Huh, D. and Paulsson, J. (2011) Non-genetic heterogeneity from stochastic partitioning at cell division. *Nat. Genet.* **43**, https://doi.org/10.1038/ng.729
10 Thomas, P. (2019) Intrinsic and extrinsic noise of gene expression in lineage trees. *Sci. Rep.* **9**, 1–16, https://doi.org/10.1038/s41598-018-35927-x
11 Hilfinger, A. and Paulsson, J. (2011) Separating intrinsic from extrinsic fluctuations in dynamic biological systems. *Proc. Natl. Acad. Sci. U.S.A.* **108**, 12167–12172, https://doi.org/10.1073/pnas.1018832108
12 Elowitz, M.B., Levine, A.J., Siggia, E.D. and Swain, P.S. (2002) Stochastic gene expression in a single cell. *Science* **297**, https://doi.org/10.1126/science.1070919
13 Cox, C.D., McCollum, J.M., Allen, M.S., Dar, R.D. and Simpson, M.L. (2008) Using noise to probe and characterize gene circuits. *Proc. Natl. Acad. Sci. U.S.A.* **105**, 10809–10814, https://doi.org/10.1073/pnas.0804829105
14 Skinner, S.O., Sepúlveda, L.A., Xu, H. and Golding, I. (2013) Measuring mRNA copy number in individual Escherichia coli cells using single-molecule fluorescent *in situ* hybridization. *Nat. Protoc.* **8**, 1100–1113, https://doi.org/10.1038/nprot.2013.066
15 Huang, H., Suslov, N.B., Li, N.S., Shelke, S.A., Evans, M.E., Koldobskaya, Y. et al. (2014) A G-quadruplex-containing RNA activates fluorescence in a GFP-like fluorophore. *Nat. Chem. Biol.* **10**, 686–691, https://doi.org/10.1038/nchembio.1561
16 Zaslaver, A., Bren, A., Ronen, M., Itzkovitz, S., Kikoin, I., Shavit, S. et al. (2006) A comprehensive library of fluorescent transcriptional reporters for Escherichia coli. *Nat. Methods* **3**, 623–628, https://doi.org/10.1038/nmeth895
17 Jahn, M., Vorpahl, C., Hübschmann, T., Harms, H. and Müller, S. (2016) Copy number variability of expression plasmids determined by cell sorting and droplet digital PCR. *Microb. Cell Fact.* **15**, 211, https://doi.org/10.1186/s12934-016-0610-8
18 De Jong, N.W., Van Der Horst, T., Van Strijp, J.A. and Nijland, R. (2017) Fluorescent reporters for markerless genomic integration in Staphylococcus aureus. *Sci. Rep.* **7**, 1–10, https://doi.org/10.1038/srep43889
19 Hautefort, I., Proença, M.J. and Hinton, J.C. (2003) Single-copy green fluorescent protein gene fusions allow accurate measurement of salmonella gene expression *in vitro* and during infection of mammalian cells. *Appl. Environ. Microbiol.* **69**, 7480–7491, https://doi.org/10.1128/AEM.69.12.7480-7491.2003
20 Lemon, K.P. and Grossman, A.D. (1998) Localization of bacterial DNA polymerase: evidence for a factory model of replication. *Science* **282**, 1516–1519, https://doi.org/10.1126/science.282.5393.1516
21 Snapp, E. (2005) Design and use of fluorescent fusion proteins in cell biology. *Curr. Protoc. Cell Biol.* **27**, 21.4.1–21.4.13, https://doi.org/10.1002/0471143030.cb2104s27
22 Chen, X., Zaro, J.L. and Shen, W.C. (2013) Fusion protein linkers: property, design and functionality. *Adv. Drug Deliv. Rev.* **65**, 1357–1369, https://doi.org/10.1016/j.addr.2012.09.039
23 Chudakov, D.M., Matz, M.V., Lukyanov, S. and Lukyanov, K.A. (2010) Fluorescent proteins and their applications in imaging living cells and tissues. *Physiol. Rev.* **90**, 1103–1163, https://doi.org/10.1152/physrev.00038.2009
24 Kremers, G.J., Goedhart, J., Van Munster, E.B. and Gadella, T.W. (2006) Cyan and yellow super fluorescent proteins with improved brightness, protein folding, and FRET Förster radius. *Biochemistry* **45**, 6570–6580, https://doi.org/10.1021/bi0516273
25 Balleza, E., Kim, J.M. and Cluzel, P. (2018) Systematic characterization of maturation time of fluorescent proteins in living cells. *Nat. Methods* **15**, 47–51, https://doi.org/10.1038/nmeth.4509

Essays in Biochemistry (2021) **65** 67–79
https://doi.org/10.1042/EBC20200015

26 Los, G.V., Encell, L.P., McDougall, M.G., Hartzell, D.D., Karassina, N., Zimprich, C. et al. (2008) HaloTag: A novel protein labeling technology for cell imaging and protein analysis. *ACS Chem. Biol.* **3**, 373–382, https://doi.org/10.1021/cb800025k

27 Young, J.W., Locke, J.C., Altinok, A., Rosenfeld, N., Bacarian, T., Swain, P.S. et al. (2012) Measuring single-cell gene expression dynamics in bacteria using fluorescence time-lapse microscopy. *Nat. Protoc.* **7**, 80–88, https://doi.org/10.1038/nprot.2011.432

28 Warren, M.R., Sun, H., Yan, Y., Cremer, J., Li, B. and Hwa, T. (2019) Spatiotemporal establishment of dense bacterial colonies growing on hard agar. *eLife* **8**, 1–47, https://doi.org/10.7554/eLife.41093

29 Blender Foundation (2020) blender.org - Home of the Blender project - free and open 3D creation software. URL: https://www.blender.org/

30 Mather, W., Mondragón-Palomino, O., Danino, T., Hasty, J. and Tsimring, L.S. (2010) Streaming instability in growing cell populations. *Phys. Rev. Lett.* **104**, 208101, https://doi.org/10.1103/PhysRevLett.104.208101

31 Ullman, G., Wallden, M., Marklund, E.G., Mahmutovic, A., Razinkov, I. and Elf, J. (2013) High-throughput gene expression analysis at the level of single proteins using a microfluidic turbidostat and automated cell tracking. *Philos. Trans. R. Soc. B Biol. Sci.* **368**, 1–8, https://doi.org/10.1098/rstb.2012.0025

32 Long, Z., Nugent, E., Javer, A., Cicuta, P., Sclavi, B., Cosentino Lagomarsino, M. et al. (2013) Microfluidic chemostat for measuring single cell dynamics in bacteria. *Lab Chip* **13**, 947–954, https://doi.org/10.1039/c2lc41196b

33 Wang, P., Robert, L., Pelletier, J., Dang, W.L., Taddei, F., Wright, A. et al. (2010) Robust growth of escherichia coli. *Curr. Biol.* **20**, 1099–1103, https://doi.org/10.1016/j.cub.2010.04.045

34 Norman, T.M., Lord, N.D., Paulsson, J. and Losick, R. (2013) Memory and modularity in cell-fate decision making. *Nature* **503**, 481–486, https://doi.org/10.1038/nature12804

35 Bakshi, S., Leoncini, E., Baker, C., Canas-Duarte, S., Okumus, B. and Paulsson, J. (2020) Tracking bacterial lineages in complex and dynamic environments with applications to growth control and persistence. *bioRxiv* 1–17, https://doi.org/10.1101/2020.03.27.006403

36 Proenca, A.M., Rang, C.U., Qiu, A., Shi, C. and Chao, L. (2019) Cell aging preserves cellular immortality in the presence of lethal levels of damage. *PLoS Biol.* **17**, 1–21, https://doi.org/10.1371/journal.pbio.3000266

37 Proenca, A.M., Rang, C.U., Buetz, C., Shi, C. and Chao, L. (2018) Age structure landscapes emerge from the equilibrium between aging and rejuvenation in bacterial populations. *Nat. Commun.* **9**, 1–11, https://doi.org/10.1038/s41467-018-06154-9

38 Li, H., Torab, P., Mach, K.E., Surrette, C., England, M.R., Craft, D.W. et al. (2019) Adaptable microfluidic system for single-cell pathogen classification and antimicrobial susceptibility testing. *Proc. Natl. Acad. Sci. U.S.A.* **116**, 10270–10279, https://doi.org/10.1073/pnas.1819569116

39 Gale, B., Jafek, A., Lambert, C., Goenner, B., Moghimifam, H., Nze, U. et al. (2018) A review of current methods in microfluidic device fabrication and future commercialization prospects. *Inventions* **3**, 60, https://doi.org/10.3390/inventions3030060

40 Wu, F. and Dekker, C. (2016) Nanofabricated structures and microfluidic devices for bacteria: From techniques to biology. *Chem. Soc. Rev.* **45**, 268–280, https://doi.org/10.1039/C5CS00514K

41 Hansen, A.S., Hao, N. and OShea, E.K. (2015) High-throughput microfluidics to control and measure signaling dynamics in single yeast cells. *Nat. Protoc.* **10**, 1181–1197, https://doi.org/10.1038/nprot.2015.079

42 Garay-Novillo, J.N., García-Morena, D., Ruiz-Masó, J.Á., Barra, J.L. and del Solar, G. (2019) Combining modules for versatile and optimal labeling of lactic acid bacteria: two pMV158-family promiscuous replicons, a pneumococcal system for constitutive or inducible gene expression, and two fluorescent proteins. *Front. Microbiol.* **10**, 1431, https://doi.org/10.3389/fmicb.2019.01431

43 Icha, J., Weber, M., Waters, J.C. and Norden, C. (2017) Phototoxicity in live fluorescence microscopy, and how to avoid it. *Bioessays* **39**, 1700003, https://doi.org/10.1002/bies.201700003

44 Lauterbach, M.A. (2012) Finding, defining and breaking the diffraction barrier in microscopy - a historical perspective. *Opt. Nanoscopy* **1**, 1–8, https://doi.org/10.1186/2192-2853-1-8

45 Otaki, T. (2000) Artifact halo reduction in phase contrast microscopy using apodization. *Opt. Rev.* **7**, 119–122, https://doi.org/10.1007/s10043-000-0119-5

46 Otaki, T. (2001) Halo reduction technique in phase contrast microscopy. *Opt. Rev.* **8**, 284–286, https://doi.org/10.1007/s10043-001-0284-1

47 Co, A.D., van Vliet, S., Kiviet, D.J., Schlegel, S. and Ackermann, M. (2020) Short-range interactions govern the dynamics and functions of microbial communities. *Nat. Ecol. Evol.* **4**, 366–375, https://doi.org/10.1038/s41559-019-1080-2

48 Garner, E.C. (2011) MicrobeTracker: quantitative image analysis designed for the smallest organisms. *Mol. Microbiol.* **80**, 577–579, https://doi.org/10.1111/j.1365-2958.2011.07580.x

49 Sliusarenko, O., Heinritz, J., Emonet, T. and Jacobs-Wagner, C. (2011) High-throughput, subpixel precision analysis of bacterial morphogenesis and intracellular spatio-temporal dynamics. *Mol. Microbiol.* **80**, 612–627, https://doi.org/10.1111/j.1365-2958.2011.07579.x

50 Paintdakhi, A., Parry, B., Campos, M., Irnov, I., Elf, J., Surovtsev, I. et al. (2016) Oufti: an integrated software package for high-accuracy, high-throughput quantitative microscopy analysis. *Mol. Microbiol.* **99**, 767–777, https://doi.org/10.1111/mmi.13264

51 Ronneberger, O., Fischer, P. and Brox, T. (2015) U-net: Convolutional networks for biomedical image segmentation. *Lecture Notes in Computer Sci. (Including Subseries Lecture Notes in Artificial Intelligence and Lecture Notes in Bioinformatics)*, vol. **9351**, pp. 234–241, Springer, Cham, https://doi.org/10.1007/978-3-319-24574-4˙28

52 Zhang, R. (2019) Making Convolutional Networks Shift-Invariant Again. In 36th International Conference on Machine Learning. *ICML* 12712–12722, (International Machine Learning Society (IMLS), 2019). 1904.11486.

53 Ester, M., Kriegel, H.-P., Sander, J. and Xu, X. (1996) A Density-Based Algorithm for Discovering Clusters in Large Spatial Databases with Noise. *Proceedings of the Second International Conference on Knowledge Discovery and Data Mining KDD'96*, pp. 226–231, AAAI Press

54 Ollion, J., Elez, M. and Robert, L. (2019) High-throughput detection and tracking of cells and intracellular spots in mother machine experiments. *Nat. Protoc.* **14**, 3144–3161, https://doi.org/10.1038/s41596-019-0216-9

55 Lugagne, J.B., Lin, H. and Dunlop, M.J. (2020) Delta: Automated cell segmentation, tracking, and lineage reconstruction using deep learning. *PLoS Comput. Biol.* **16**, 1–18, https://doi.org/10.1371/journal.pcbi.1007673
56 Ollion, J. and Ollion, C. (2020) DistNet: Deep Tracking by displacement regression: application to bacteria growing in the Mother Machine. In *Medical Image Computing and Computer Assisted Intervention – MICCAI 2020. MICCAI 2020. Lecture Notes in Computer Science* (Martel, A.L., ed.), vol. **12265**, Springer, Cham, https://doi.org/10.1007/978-3-030-59722-1˙21
57 Sauls, J., Schroeder, J., Brown, S., Treut, G.L., Si, F., Li, D. et al. (2019) Mother machine image analysis with MM3. *bioRxiv* 10.1101/ 810036
58 Smith, A., Metz, J. and Pagliara, S. (2019) MMHelper: an automated framework for the analysis of microscopy images acquired with the mother machine. *Sci. Rep.* **9**, 1–12, https://doi.org/10.1038/s41598-019-46567-0
59 Kaiser, M., Jug, F., Julou, T., Deshpande, S., Pfohl, T., Silander, O.K. et al. (2018) Monitoring single-cell gene regulation under dynamically controllable conditions with integrated microfluidics and software. *Nat. Commun.* **9**, 1–16, https://doi.org/10.1038/s41467-017-02505-0
60 Jug, F., Pietzsch, T., Kainmüller, D., Funke, J., Kaiser, M., van Nimwegen, E. et al. (2014) Optimal joint segmentation and tracking of escherichia coli in the mother machine. *Lecture Notes in Computer Science (Including Subseries Lecture Notes in Artificial Intelligence and Lecture Notes in Bioinformatics)* **8677**, 25–36
61 Lichtner, G. (2021) glichtner/pystackreg: a python extension for the automatic alignment of a source image or a stack (movie) to a target image/reference frame. URL: https://github.com/glichtner/pystackreg
62 Mathworks (2021) Register images using registration estimator app - MATLAB I& Simulink. URL: https://www.mathworks.com/help/images/register-images-using-the-registration-estimator-app.html
63 Thévenaz, P., Ruttimann, U.E. and Unser,, M. (1998) A pyramid approach to subpixel registration based on intens. *IEEE Transactions on Image Processing* **7**, 27–41, URL: http://bigwww.epfl.ch/thevenaz/stackreg/, https://doi.org/10.1109/83.650848
64 Kozubek, M. and Matula, P. (2000) An efficient algorithm for measurement and correction of chromatic aberrations in fluorescence microscopy. *J. Microsc.* **200**, 206–217, https://doi.org/10.1046/j.1365-2818.2000.00754.x
65 Born, M., Wolf, E., Bhatia, A.B., Clemmow, P.C., Gabor, D. and Stokes, A.R. (1999) *Principles of Optics*, Cambridge University Press
66 Kirshner, H., Sage, D. and Unser, M. (2011) 3D PSF Models for Fluorescence Microscopy in ImageJ. *Proceedings of the Twelfth Int. Conference on Methods and Applications of Fluorescence Spectroscopy, Imaging and Probes (MAF'11)*, p. 154, AAAI Press, Strasbourg, French Republic
67 Golding, I., Paulsson, J., Zawilski, S.M. and Cox, E.C. (2005) Real-time kinetics of gene activity in individual bacteria. *Cell* **123**, 1025–1036, https://doi.org/10.1016/j.cell.2005.09.031
68 Rosenfeld, N., Perkins, T.J., Alon, U., Elowitz, M.B. and Swain, P.S. (2006) A fluctuation method to quantify in vivo fluorescence data. *Biophys. J.* **91**, 759–766, https://doi.org/10.1529/biophysj.105.073098